Indirect heating of Pt by short-pulse laser irradiation of Au in a nanoscale Pt/Au bilayer

Gyung-Min Choi,* R. B. Wilson, and David G. Cahill

Department of Materials Science and Engineering and Materials Research Laboratory, University of Illinois, Urbana, Illinois 61801, USA

(Received 18 July 2013; revised manuscript received 2 February 2014; published 24 February 2014)

Thermal transport in a metallic multilayer on picosecond time scales is controlled by the electronic thermal conductivity (Λ_e), the electronic interfacial thermal conductance (G_{ee}), and electron-phonon coupling constant (g). We analyze heat transfer in a nanoscale Pt/Au bilayer using data obtained in pump-probe measurements and modeling using a transmission-line-equivalent circuit. For optical exciation of either the Pt or Au side of the bilayer, the majority of energy is deposited into the Pt phonons on a time scale of $\approx$1 ps because $g_{\mathrm{Pt}} \gg g_{\mathrm{Au}}$ and $G_{ee} > g_{\mathrm{Au}} h_{\mathrm{Au}}$, where h_{Au} is the thickness of the Au layer. We determine g of the Au layer and set a lower bound on G_{ee} of the Pt/Au interface: $g_{\mathrm{Au}} = 2.2 \pm 0.6 \times 10^{16}$ W m^{-3} K^{-1} and $G_{ee} > 5$ GW m^{-2} K^{-1}.

DOI: 10.1103/PhysRevB.89.064307 PACS number(s): 66.70.Df

I. INTRODUCTION

When an ultrafast optical pulse is absorbed by a thin metal film, energy is initially deposited into the electronic excitations, which are then driven out of thermal equilibrium with the vibrations of the atomic lattice [1]. The rate of equilibration of electrons and phonons in a homogeneous metal layer has been extensively studied [2–8]. Recently, we described the relatively slow thermal equilibration of a metal bilayer where one component of the bilayer with strong electron-phonon coupling (Pt) was used to indirectly heat a second component of the bilayer that has weak electron-phonon coupling (Au) [8].

The focus of our current study is the reverse: we wish to better understand the indirect heating of a thin layer with strong electron-phonon coupling (Pt) when in contact with an optically excited layer with weak electron-phonon coupling (Au). Regardless of whether the pump pulse heats the bilayer from the Pt side or the Au side of the bilayer, the majority of the energy of the pump pulse is deposited into the phonons of Pt on short time scales of $t \approx 1$ ps. The effect of weak electron-phonon coupling on the initial energy distribution in multilayers has been investigated previously through modeling and simulation [9–11] and in experiments that reported a reduction in the temperature of a laser-heated Au film in the presence of a V sublayer [12].

At short time scales, thermal transport in a metallic multilayer is governed by the electronic thermal conductivity (Λ_e) of each layer, the strength of electron-phonon coupling (g) in each layer, and the electronic thermal conductance (G_{ee}) of the interface. Since Λ_e, G_{ee}, and g have different units, we examine effective thermal conductances to gain insight about which parameters are most important. The electronic thermal conductance of each layer is the thermal conductivity divided by the layer thickness, Λ_e/h. The effective thermal conductance due to electron-phonon coupling is gd, where d is the characteristic length over which the electrons and phonons have different temperatures. At short time scales in a single thick metal film, d is the heat diffusion length, $d \approx \sqrt{\tau D_e}$, where $D_e = \Lambda_e/C_e$ is the thermal diffusivity of electrons and $\tau = C_e/g$ is the time required for the electrons and phonons to thermalize. In a metal bilayer with a large value of G_{ee}, the electron temperature profiles of each layer are interdependent and $\tau > C_e/g$ [8]. Therefore, for a thick film in a bilayer system, d is higher than $\sqrt{\Lambda_e/g}$ and $\sqrt{\Lambda_e g}$ is a lower bound on the effective electron-phonon conductance in the thick film. For thin layers, i.e., $h \ll \sqrt{\Lambda_e/g}$, the effective electron-phonon conductance is gh. In the sample we are studying, the Pt layer is in the thick limit, while the Au layer is better approximated by the thin-film limit. Values for the electronic thermal conductance and the electron-phonon conductance for the Au and Pt layers are summarized in Table I.

One of the original goals of our work was to determine G_{ee}, the electronic thermal conductance of the Pt/Au interface. Because of the large value of G_{ee}, however, we were not able to design an experiment with sufficient sensitivity to reliably determine G_{ee} and are only able to set a lower limit. The sensitivity to G_{ee} is poor because the more important conductances in the problem—the effective electron-phonon conductance of Au and the electronic thermal conductance of the Pt layer—are relatively small, $\approx$2 GW m^{-2} K^{-1}. These small conductances are more important for controlling thermal transport in the bilayer than the thermal conductance of the Pt/Au interface.

To make the analysis as quantitative as possible, we analyze thermal transport in the bilayer using a transmission-line circuit model. The circuit model is a discretized version of the two temperature model (TTM) [9]. We use the circuit model because it is easier to solve than the continuum TTM equation, where the electronic heat capacity, electronic thermal conductivity, and electronic thermal conductance depend on temperature. The discretized model should give the same result as the continuum model as long as the discrete length scale is sufficiently small.

We determine g_{Au} and a lower bound for G_{ee}. We find $g_{\mathrm{Au}} = 2.2 \pm 0.6 \times 10^{16}$ W m^{-3} K^{-1} and $G_{ee} > 5$ GW m^{-2} K^{-1}. Reported values of g_{Au} extend from 2 to 4 $\times$ 10^{16} W m^{-3} K^{-1}: Hohlfeld *et al.* reported $2.1 \pm 0.3 \times 10^{16}$ W m^{-3} K^{-1} by measuring the Au electron temperature of an Au film [6]; Wang and Cahill reported 2.8×10^{16} W m^{-3} K^{-1} by measuring the Pt phonon temperature of a Pt/Au bilayer [8]; and Lin *et al.* reported 2.6×10^{16} W m^{-3} K^{-1} from a first-principles calculation [1]. The lower bound of G_{ee} is consistent with the conductance predicted by the diffuse-mismatch model for electrons [13,14] and the conductance predicted by applying the Wiedemann-Franz law to measurements of the specific electrical resistance of analogous Pt/Cu and Pd/Au interfaces [15–17].

*Corresponding author: gchoi11@illinois.edu

TABLE I. Parameters for the thermal modeling of the sapphire substrate/Pt/Au structure in Fig. 3. C_{total} is the total heat capacity, γ is the electronic heat capacity coefficient, Λ_e is electronic thermal conductivity at room temperature, Λ_{ph} is phonon thermal conductivity, and g is the electron-phonon coupling parameter. In addition we set G_{ph}, the phonon thermal conductance, to 0.1 GW m^{-2} K^{-1} for both sapphire/Pt and Pt/Au interfaces. The electron-phonon coupling parameter of Au and electronic thermal conductance at Pt/Au interface are free parameters.

	Sapphire	Pt	Au
C_{total} (10^6 J m^{-3} K^{-1})	3.08[a]	2.85[a]	2.49[a]
γ (J m^{-3} K^{-2})		750[b]	68[b]
Λ_e (W m^{-1} K^{-1})		50[c]	200[c]
Λ_{ph} (W m^{-1} K^{-1})	30[d]	7[e]	3[f]
g (10^{16} W m^{-3} K^{-1})		110[g]	
Λ_e/h (10^9 W m^{-2} K^{-1})		2.2	3.4
gh (10^9 W m^{-2} K^{-1})		25	1.3
$\sqrt{\Lambda_e g}$ (10^9 W m^{-2} K^{-1})		7.4	2.1

[a]Reference [26].
[b]Reference [27].
[c]Obtained from electrical conductivity and the Wiedemann-Franz law.
[d]Obtained as fitting parameters for thermal analysis.
[e]Reference [28].
[f]Reference [29].
[g]Reference [7].

An additional motivation for our work is to correct what we believe is an error in the literature. Eschenlohr *et al*. observed that excitation of an Au layer in an Au/Ni bilayer by an ultrafast laser pulse produces nearly the same demagnetization of a Ni layer as heating the Ni layer directly [18]. The authors of Ref. [18] excluded the effect of heat transport in their analysis of the experiment because they assumed that the time scale for heat transport between Au and Ni is much slower than the observed time scale, ≈0.5 ps, of demagnetization of the Ni layer. Our work shows that rapid, indirect heating of magnetic layers due to fast electronic thermal transport and small electron-phonon coupling in Au should be taken into account in analyzing experiments of the type described in Ref. [18].

II. EXPERIMENTAL DETAILS

The structure of the sample we studied is a sapphire substrate coated sequentially by 23 nm of Pt and 58 nm of Au by magnetron sputter deposition at room temperature with a working pressure of 2 mTorr. The base pressure of the deposition chamber is $<5 \times 10^{-8}$ Torr. We used x-ray reflectivity to measure the thicknesses of the Pt and Au layers. After measuring the total thickness of the Pt/Au bilayer, we removed the Au layer using a KI/I_2-based etchant and measured the thickness of the remaining Pt layer. Electric conductivities of the Pt and Au layer are measured using a four-point probe: 6.3×10^6 Ω^{-1} m^{-1} for Pt and 2.7×10^7 Ω^{-1} m^{-1} for Au. We used ellipsometry to measure the complex refractive indexes of Pt and Au using a 100-nm-thick Pt film and a 200-nm-thick Au film deposited on a sapphire substrate: $2.67 + i5.94$ for Pt and $0.15 + i4.90$ for Au at a wavelength of 785 nm.

The temperature response of the Pt and Au layers to abrupt heating is measured by time-domain thermoreflectance (TDTR) using a Ti-sapphire laser that operates at a wavelength near 785 nm [19]. All measurements are performed at room temperature. The reflectivity change includes contributions from both electron and phonon temperatures, $\Delta R = a\Delta T_e + b\Delta T_{\text{ph}}$, but the dominant contribution comes from phonon temperature unless the electron temperature excursion is very high; by comparing our experiments and models, we estimate $a/b \approx 0.25$ for Pt and $a/b \approx 0.02$ for Au.

We use a double modulation technique with the pump beam modulated at 9.8 MHz and the probe beam modulated at 200 Hz to improve the signal-to-noise and suppress background created by a diffusely scattered pump light. To a good approximation at high modulation frequencies, the in-phase signal of the lock-in amplifier $V_{\text{in}}(t)$ is proportional to the time-domain thermal response of the sample, i.e., the temperature excursion created by each pump-optical pulse. The out-of-phase signal $V_{\text{out}}(t)$ is mostly determined by the imaginary part of the frequency domain response at the modulation frequency and is approximately independent of delay time. A complete description of the analysis of TDTR data and the interpretation of V_{in} and V_{out} can be found in Ref. [19]. For the purpose of this work, we interpret the ratio $|V_{\text{in}}/V_{\text{out}}|$ as the temperature excursion normalized by the amount of energy absorbed per pulse.

To take into account the large difference in reflectivity, $R = 0.66$ at the sapphire/Pt interface compared to $R = 0.972$ at the Au surface, we use 12 times higher pump pulse energy (E) for the Au side than for the Pt side. The $1/e^2$ intensity radius of the pump and probe beams is $w = 5$ μm. Therefore, the average fluence of energy absorbed is $F = (1 - R)E/(\pi w^2) \approx 1.6$ J m^{-2} per pulse in both cases. At this laser fluence, the electron-phonon coupling parameter, g, of Pt and Au is independent of temperature [1].

We set the zero time delay of all measurements to the midpoint of the initial rise of the TDTR signal. For the modeling, we set the zero time delay to the midpoint of the pump pulse. When the pump beam is incident on the sapphire/Pt interface, we use our standard two-tint approach [20] of using optical filters to spectrally separates the center wavelengths of the pump and probe beam by ≈6 nm. In this case, the duration of the pump pulses is ≈0.4 ps. When the pump beam is incident on the Au surface, we omit the optical filters to obtain larger optical power. In this case, the duration of the pump-optical pulses is significantly broadened to full-width at half maximum (FWHM) ≈ 0.8 ps by the large dispersion of the electro-optic modulator [20].

III. RESULTS AND DISCUSSION

To determine the initial energy distribution into the electronic system, we calculate the light absorption as a function of depth in the Pt/Au bilayer using a transfer matrix method [Fig. 1(a)]. When laser light is incident on the Pt/sapphire interface, 99% of the energy is absorbed by the 23-nm-thick Pt layer and the rest (1%) by the 58-nm-thick Au layer. When the laser light is incident on the Au surface, 85% of the energy

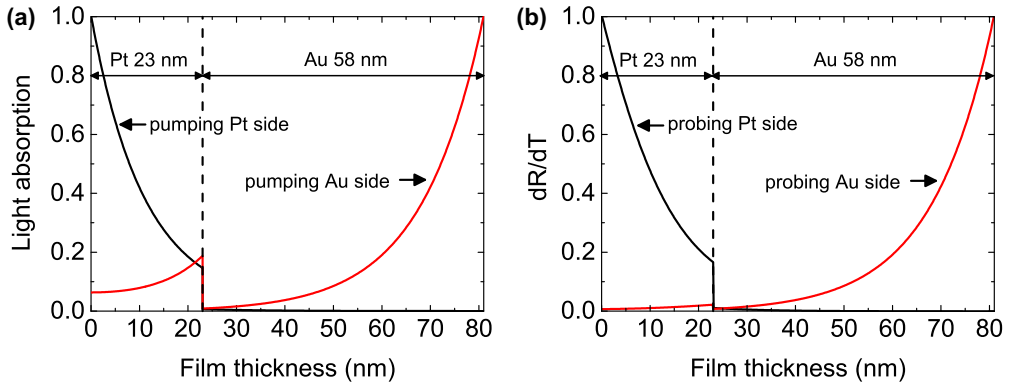

FIG. 1. (Color online) (a) The distribution of light absorption as a function of depth in the Pt (23)/Au (58) bilayer. The calculation is done by a transfer matrix method with refractive indexes of Pt and Au, $2.67 + i5.94$ and $0.15 + i4.90$, respectively. The light absorption for the pump-beam incident on the Pt/sapphire interface is shown as a black line and that for the pump beam incident on the Au surface is shown as a red line. (b) The reflectance (dR/dT) weighting factor of the Pt (23)/Au (58) bilayer. The calculation is done by the transfer matrix method with refractive indexes as well as temperature coefficients of those, $dn_{\rm Pt}/dT = 2.6 \times 10^{-4}$ K^{-1}, $dk_{\rm Pt}/dT = -3 \times 10^{-4}$ K^{-1}, $dn_{\rm Au}/dT = 2 \times 10^{-4}$ K^{-1}, and $dk_{\rm Au}/dT = 0$. The black solid line corresponds to when light is incident on the Pt side, and the red solid line corresponds to when light is incident on the Au side.

is absorbed by the 58-nm-thick Au layer and the rest (15%) by the 23-nm-thick Pt layer.

In a TDTR measurement, the measured signal is a weighted average of the temperature-profile through depths below the surface [21]. The weighting function extends over a distance that is approximately the same as the optical attenuation depth and is calculated from an optical model for dR/dT vs film depth using the previously reported [22] temperature coefficients of refractive indexes of Pt and Au: $dn_{\rm Pt}/dT = 2.6 \times 10^{-4}$ K^{-1}, $dk_{\rm Pt}/dT = -3 \times 10^{-4}$ K^{-1}, $dn_{\rm Au}/dT = 2 \times 10^{-4}$ K^{-1}, and $dk_{\rm Au}/dT = 0$ [Fig. 1(b)].

We model thermal transport in the Pt/Au bilayer using an equivalent circuit. Figure 2 shows a schematic of the approach, where the five capacitors represent the heat capacities for Pt electrons ($C_{e\_{\rm Pt}}$), Au electrons ($C_{e\_{\rm Au}}$), Pt phonons ($C_{\rm ph\_Pt}$), Au phonons ($C_{\rm ph\_Au}$), and sapphire phonons ($C_{\rm ph\_sap}$), respectively; the five resistors represent electron-phonon coupling of Pt ($g_{\rm Pt}$), electron-phonon coupling of Au ($g_{\rm Au}$), the electronic thermal conductance of the Pt/Au interface (G_{ee}), the phonon thermal conductance of the Pt/Au interface ($G_{\rm ph\_Pt/Au}$), and the phonon thermal conductance of the sapphire/Pt interface ($G_{\rm ph\_sap/Pt}$).

$$C_1 = C_{e\_{\rm Pt}} A h_{\rm Pt} \quad C_2 = C_{e\_{\rm Au}} A h_{\rm Au} \quad C_3 = C_{\rm ph\_Pt} A h_{\rm Pt}$$
$$C_4 = C_{\rm ph\_Au} A h_{\rm Au} \quad C_5 = C_{\rm ph\_sap} A h_{\rm sap}$$
$$R_1 = \frac{1}{A h_{\rm Pt} g_{\rm Pt}} \quad R_2 = \frac{1}{A h_{\rm Au} g_{\rm Au}} \quad R_3 = \frac{1}{A G_{ee}}$$
$$R_4 = \frac{1}{A G_{\rm ph\_Pt/Au}} \quad R_5 = \frac{1}{A G_{\rm ph\_sap/Pt}},$$

where A is the area and h is the thickness. Excitation by the pump beam is represented by the current sources $I1$ and $I2$ that are connected to Pt and Au electrons, respectively. Voltages of each capacitor represent the temperature excursions of each heat reservoir.

To model the thermal transport within each layer, the individual layers that are demarcated by blue dashed lines in Fig. 2(a) are divided into multiple sublayers [Fig. 2(b)]. In other words, we divide the single capacitors of each layer into multiple subcapacitors and connect them with resistors that represent thermal resistance by electronic thermal conductivity, phonon thermal conductivity, and electron-phonon coupling,

$$C_{\rm sub} = C A h_{\rm sub} \quad R_{ee} = \frac{h_{\rm sub}}{A \Lambda_e}$$
$$R_{pp} = \frac{h_{\rm sub}}{A \Lambda_{\rm ph}} \quad R_{ep} = \frac{1}{A h_{\rm sub} g},$$

where $h_{\rm sub}$ is the sublayer thickness, Λ_e is the electronic thermal conductivity, and $\Lambda_{\rm ph}$ is the phonon thermal conductivity. We use 2 nm and 10 nm for the thickness of the sublayers of the Pt and Au layers, respectively. For both Pt and Au, these thicknesses are several times smaller than the characteristic length scale for electron-phonon coupling, $\sqrt{\Lambda_e/g}$. We also confirmed that the final result does not change when the sublayer thicknesses are less 6 nm and 30 nm, respectively, for the Pt and Au layers.

To model the pump-pulse incident on the Pt side or Au side, we partition the current in $I1$ and $I2$ according to a transfer matrix calculation of the optical absorption. Inside each layer, we also distribute the current into the sublayers with an attenuation length of $\approx$11 nm for Pt and $\approx$13 nm for Au, as illustrated by Fig. 1(a). To model optical pumping of the Pt side, the shape of the current pulse is a trapezoid with a rise time of 0.2 ps, pulse width of 0.2 ps, and fall time of 0.2 ps; this trapezoidal shaped current pulse has the same FWHM of 0.4 ps as the spectrally narrowed pump-optical pulses in the two-tint approach [20]. To model optical pumping of the Au side, the time scales of the trapezoidal current pulse are doubled to produce a FWHM of 0.8 ps.

To model the thermoreflectance measured by the probe pulse incident on the Pt side or Au side, we sum the calculated temperatures of sublayers by the weighting function of Fig. 1(b) that represents the relative contribution of each sublayer to the change in reflectivity.

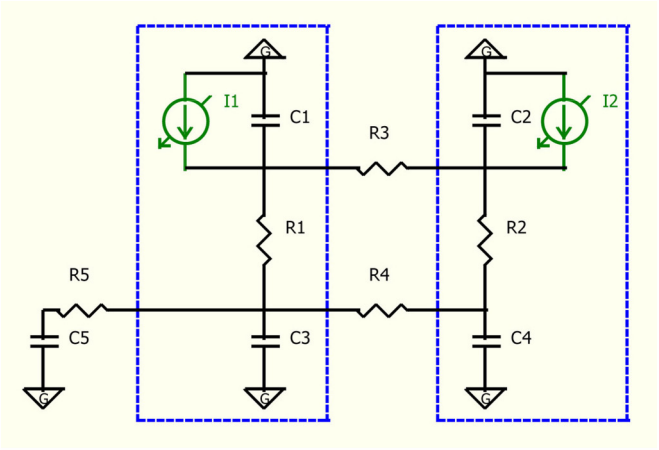

(a)

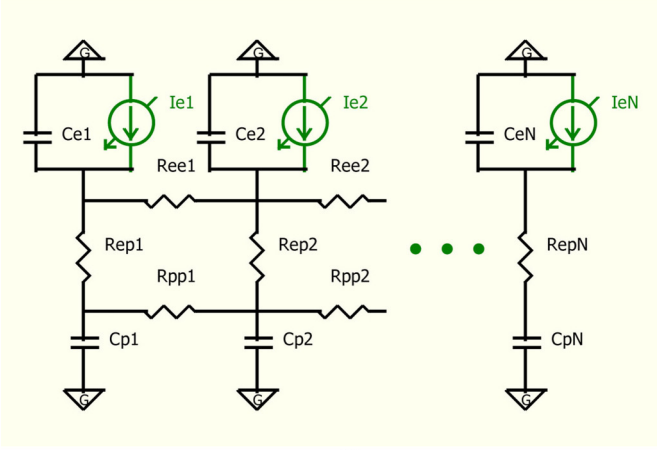

(b)

FIG. 2. (Color online) (a) Equivalent circuit for modeling the thermal transport between the Pt/Au bilayer. C, R, and I represent capacitors, resistors, and current source, respectively. $C1$ and $C2$ represent the electronic heat capacities of the Pt and Au layers. $C3$, $C4$, and $C5$ represent the corresponding lattice heat capacities of the Pt, Au, and sapphire layers; $R1$ and $R2$ represent the thermal resistances due to the electron-phonon coupling of the Pt and Au layers; $R3$ represents the thermal resistance due to the electronic thermal conductance of the Pt/Au interface; $R4$ and $R5$ represent the thermal resistances due to the phonon thermal conductance of the Pt/Au and sapphire/Pt interfaces, respectively; and $I1$ and $I2$ represent the current sources, which mimic the excitation of electrons of the Pt and Au layers by the pump-optical pulse. (b) Transmission line model for each layer, which is indicated as blue dotted line in (a). Ce and Cp represent the heat capacities of electrons and phonons, respectively, of each sublayer; Ree and Rpp represent the thermal resistances due to electronic and phonon, respectively, thermal conductivities between sublayers; Rep represents the thermal resistance due to electron-phonon coupling of the sublayer; and Ie, the current source, represents the excitation of electrons of the sublayer by the pump optical pulse.

Because the excursion of the electron temperature at short time scales significantly exceeds room temperature, we include the temperature dependence of the electronic heat capacity, $C_e = \gamma T_e$, the electronic thermal conductivity, $\Lambda_e = \kappa T_e$, and the electronic interface thermal conductance, $G_{ee} = \Gamma \langle T_e \rangle$,

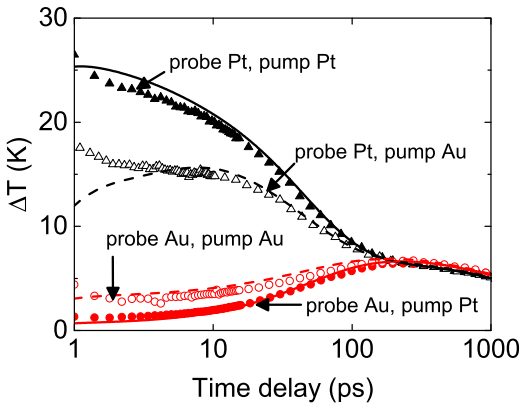

FIG. 3. (Color online) Time-domain thermoreflectance (TDTR) data of the sapphire/Pt (23)/Au (58) sample with four different configurations of the pump and probe beams: (i) pump and probe at the Pt side of the bilayer (▲); (ii) pump at Au surface and probe at the Pt side (Δ); (iii) pump at the Pt side and probe at the Au surface (●); and (iv) pump and probe at the Au surface (○). Solid and dashed lines are from the thermal modeling with $g_{\mathrm{Au}} = 2.2 \times 10^{16}$ W m^{-3} K^{-1} and $\Gamma = 50$ MW m^{-2} K^{-2}; black lines are for Pt phonon temperatures, and red lines are for Au phonon temperatures. Solid lines are for the pump-beam incident on the Pt side of the bilayer, and dashed lines are for the pump-beam incident on the Au surface.

where $\langle T_e \rangle$ represents the average electronic temperature at the Pt/Au interface. The assumption of a linear temperature dependence of Λ_e is based on the argument that the phonon- and defect-scattering rates of electrons should be relatively insensitive to electronic temperature; therefore, the dependence of the thermal conductivity on electronic temperature should scale with the heat capacity of the electronic system. The assumption of a linear dependence of G_{ee} on electronic temperature is based on the diffuse mismatch model for electrons [13].

Figure 3 shows TDTR data collected for all four permutations of the placement of the pump and probe; the pump and probe beams can be incident at either the Pt side of the bilayer or the Au surface. Regardless of the pump-beam location, the Pt phonon temperature is higher than the Au phonon temperature: most of the energy in the pump beam is deposited into the Pt phonons at short delay times even when pump beam is incident on the Au side of the bilayer. As discussed above, this result is due to the large difference in the strength of electron-phonon coupling in Pt and Au and the fact that the electronic thermal conductivity and thermal conductance are large enough to effectively couple the temperatures of the electrons of the Pt and Au layers.

Using the transmission-line circuit model, we can reproduce data for all four pump-probe configurations over the entire time scale from 2 to 1000 ps. The two free parameters in the modeling are the electron-phonon coupling parameter of Au, g_{Au}, and electronic thermal conductance of Pt/Au interface, $G_{ee} = \Gamma \langle T_e \rangle$. In Fig. 3, we show a fit to the experimental data with $g_{\mathrm{Au}} = 2.2 \times 10^{16}$ W m^{-3} K^{-1} and $\Gamma = 50$ MW m^{-2} K^{-2}: g_{Au} is chosen by minimizing the deviation between data and modeling in Fig. 4(a) and Γ is chosen where the deviation approaches the minimum value as a function of Γ, as shown in Fig. 4(b).

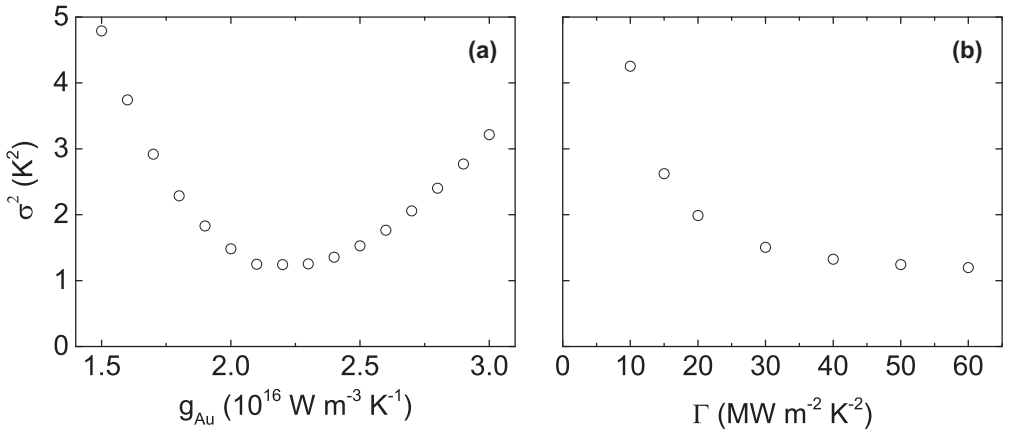

FIG. 4. The mean square deviation, σ^2, between experiment and modeling in time scale from 2 to 200 ps: (a) varying g_{Au} while fixing $\Gamma = 50$ MW m^{-2} K^{-2}; (b) varying Γ while fixing $g_{\mathrm{Au}} = 2.2 \times 10^{16}$ W m^{-3} K^{-1}.

Table I summarizes parameters used in the thermal model. The phonon thermal conductivity of sapphire substrate and the phonon thermal conductance of the sapphire/Pt interface are determined by independently fitting the thermoreflectance data at long delay times, 0.2 to 1 ns. The electronic thermal conductivities of Pt and Au are estimated by applying the Wiedemann-Franz law to the measured in-plane electrical conductivity. The phonon thermal conductivity of metallic layers and phonon thermal conductance of the Pt/Au has a negligible effect on calculation. The major sources of error propagation are the uncertainties in the thicknesses of $\approx$5% and uncertainties in Λ_e that we estimate as $\approx$10%. Measurements from the Pt side of the bilayer include a systematic error created by the temperature variations of the index of refraction of the sapphire substrate. We estimate the size of this systematic error in the ratio signal as $\approx$4% based on optical modeling of the reflectivity of the Pt/sapphire interface with and without a temperature excursion in the sapphire substrate.

In Fig. 4, we show a calculation of the mean of the square of the deviation between the experiment and modeling as a function of the choices for the values of g_{Au} and Γ.

$$\sigma^2 = \sum_{j=1}^{4} \frac{\sum_{i=1}^{n} (T_{d,i} - T_{m,i})^2}{n},$$

where $T_{d,i}$ and $T_{m,i}$ are the temperature of the TDTR data and the modeling, respectively, at each time delay; n is the total number of time delays; and j is an index that denotes each of the four pump-probe configurations.

Setting upper and lower bounds to when the mean square deviation becomes twice that of the minimum value, we determine $g_{\mathrm{Au}} = 2.2 \pm 0.6 \times 10^{16}$ W m^{-3} K^{-1}. Previously reported values of g_{Au} fall within the range of 2 to 4×10^{16} W m^{-3} K^{-1} [1–6,8]. For Γ, only a lower bound exists because electronic thermal transport has little sensitivity on Γ when Γ becomes large. The mean square deviation becomes twice as large as the minimum value at $\Gamma = 15$ MW m^{-2} K^{-2}. At room temperature this value for Γ leads to the lower bound, $G_{ee} > 5$ GW m^{-2} K^{-1}.

A prediction of G_{ee} has been described by an extension of the diffusive-mismatch model (DMM) [23]. The electronic version of DMM leads to the following expression for Γ [13]:

$$\Gamma = \frac{1}{4} \frac{v_{1F}\gamma_1 v_{2F}\gamma_2}{v_{1F}\gamma_1 + v_{2F}\gamma_2},$$

where γ is the electronic heat capacity coefficient and v_F is the Fermi velocity. Using $v_F = 0.24 \times 10^6$ m sec^{-1} for the [111] direction of Pt [24] and $v_F = 1.4 \times 10^6$ m sec^{-1} from the free-electron model for Au, the DMM prediction for Γ is 15.5 MW m^{-2} K^{-2}, i.e., $G_{ee} \approx 5$ GW m^{-2} K^{-1} at room temperature. We have previously shown that the Wiedemann-Franz law works well in predicting the thermal conductance of Pd/Ir interfaces [14]. Previous reports on specific electrical resistance, AR, of analogous interfaces combined with the Wiedemann-Franz law predicts $G_{ee} \approx 10$ GW m^{-2} K^{-1} for Pt/Cu and $G_{ee} \approx 30$ GW m^{-2} K^{-1} for Pd/Au interfaces [15–17]. These results are consistent with our experimental lower limit, $G_{ee} > 5$ GW m^{-2} K^{-1}.

Even for the best fit, the TDTR data deviate from the model at the short time scale. At less than 2 ps, deviation from the phonon temperatures and measured TDTR data can be explained by the large temperature excursion of the electrons, invalidating our assumption that the measured signal is dominated by the phonon temperature contribution. The smaller deviation from 2 to 10 ps between the TDTR data and the predicted Pt and Au phonon temperatures suggests that the initial energy distribution extends further than the optical calculation of Fig. 1(a). Hohlfeld *et al.* reported that the energy absorption depth can be enhanced by nonthermal-ballistic motion of electrons [6]. This effect is not included in our transmission line model.

Finally, in Fig. 5, we show the time evolution of both the electron and phonon temperatures of the Pt and Au layers. The temperature is obtained by averaging temperatures of the Pt and Au sublayers of the modeling without a weighting factor. The behavior of the electron and phonon temperatures of the Pt layer are comparable whether the pump beam is incident on the Pt side or Au side of the bilayer. When the pump beam is incident on the Au surface, the peak electron temperature of Pt layer reaches 57% of that of pumping the Pt side, and the time delays of the peak electron temperatures differ by less than 0.2 ps. Ni has a similar electron-phonon coupling parameter with Pt [7], and the demagnetization of

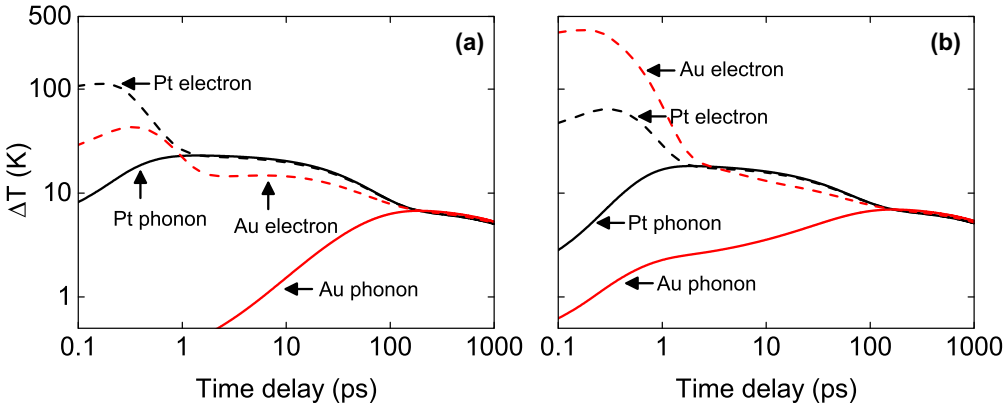

FIG. 5. (Color online) The average electron and phonon temperature excursions of the sapphire/Pt (23)/Au (58) sample calculated from the thermal model with $g_{Au} = 2.2 \times 10^{16}$ W m^{-3} K^{-1} and $\Gamma = 50$ MW m^{-3} K^{-2} when pump beam excites the Pt side (a) or the Au side (b) of the Pt/Au bilayer; black lines are for Pt temperature, and red lines are Au temperature. Solid lines are for phonon temperature, and dashed lines are for the electron temperature. The average pump fluence and FWHM are fixed to 1.6 J m^{-2} and 0.4 ps, respectively, in both (a) and (b).

a metallic ferromagnet is strongly affected by its electron and phonon temperature [25]. Therefore, we argue that the ultrafast demagnetization of the Ni layer by exciting Au side in the Au (30)/Ni (15) structure in Ref. [18] is probably due to fast electronic thermal transport between Au and Ni and slow electron-phonon equilibration in Au, which were not considered in the analysis of Ref. [18].

IV. CONCLUSIONS

We have shown that a nanoscale layer with strong electron-phonon coupling is indirectly heated by the electronic excitations of an optically excited nanoscale layer with weak electron-phonon coupling. This indirect heating is highly efficient: the electronic temperature excursion of a 23-nm Pt layer created by the electronic heat transfer from an adjacent 58-nm Au layer is 57% of that created by directly heating the Pt layer. The electronic thermal conductance of the Pt/Au interface is large and does not significantly limit the heat transfer. This indirect heating effect should be considered in the analysis of thermal transport in metallic multilayers whenever one of the layers has relatively weak electron-phonon coupling.

ACKNOWLEDGMENTS

This work was supported by the U.S. Department of Energy Office of Basic Energy Sciences under Grant No. DE-FG02-07ER46459 and was carried out in the Laser and Spectroscopy Laboratory of the Materials Research Laboratory at the University of Illinois Urbana-Champaign. We acknowledge Xuan Zhang and Robert S. Averback at UIUC for help in the sample preparation.

[1] Z. Lin, L. V. Zhigilei, and V. Celli, Phys. Rev. B **77**, 075133 (2008).
[2] S. D. Brorson, A. Kazeroonian, J. S. Moodera, D. W. Face, T. K. Cheng, E. P. Ippen, M. S. Dresselhaus, and G. Dresselhaus, Phys. Rev. Lett. **64**, 2172 (1990).
[3] H. E. Elsayed-Ali, T. Juhasz, G. O. Smith, and W. E. Bron, Phys. Rev. B **43**, 4488 (1991).
[4] R. H. M. Groeneveld, R. Sprik, and A. Lagendijk, Phys. Rev. B **51**, 11433 (1995).
[5] J. L. Hostetler, A. N. Smith, D. M. Czajkowsky, and P. M. Norris, Appl. Opt. **38**, 3614 (1999).
[6] J. Hohlfeld, S.-S. Wellershoff, J. Güdde, U. Conrad, V. Jähnke, and E. Matthias, Chem. Phys. **251**, 237 (2000).
[7] A. P. Caffrey, P. E. Hopkins, J. M. Klopf, and P. M. Norris, Microscale Thermophys. Eng. **9**, 365 (2005).
[8] W. Wang and D. G. Cahill, Phys. Rev. Lett. **109**, 175503 (2012).
[9] T. Q. Qiu and C. L. Tien, Int. J. Heat Mass Transfer **37**, 2789 (1994).
[10] D. A. Thomas, Z. Lin, L. V. Zhigilei, E. L. Gurevich, S. Kittel, and R. Hergenröder, Appl. Surf. Sci. **255**, 9605 (2009).
[11] C. Wu, D. A. Thomas, Z. Lin, and L. V. Zhigilei, Appl. Phys. A **104**, 781 (2011).
[12] W. M. G. Ibrahim, H. E. Elsayed-Ali, C. E. Bonner, Jr., and M. Shinn, Int. J. Heat Mass Transfer **47**, 2261 (2004).
[13] B. C. Gundrum, D. G. Cahill, and R. S. Averback, Phys. Rev. B **72**, 245426 (2005).
[14] R. B. Wilson and D. G. Cahill, Phys. Rev. Lett. **108**, 255901 (2012).
[15] W. P. Pratt, Jr. and J. Bass, Appl. Surf. Sci. **256**, 399 (2009).
[16] H. Kurt, R. Loloee, K. Eid, W. P. Pratt, Jr., and J. Bass, Appl. Phys. Lett. **81**, 4787 (2002).
[17] C. Galinon, K. Tewolde, R. Loloee, W.-C. Chiang, S. Olson, H. Kurt, W. P. Pratt, Jr., J. Bass, P. X. Xu, Ke Xia, and M. Talanana, Appl. Phys. Lett. **86**, 182502 (2005).
[18] A. Eschenlohr, M. Battiato, P. Maldonado, N. Pontius, T. Kachel, K. Holldack, R. Mitzner, A. Föhlisch, P. M. Oppeneer, and C. Stamm, Nature Materials **12**, 332 (2013).
[19] D. G. Cahill, Rev. Sci. Instrum. **75**, 5119 (2004).
[20] K. Kang, Y. K. Koh, C. Chiritescu, X. Zheng, and D. G. Cahill, Rev. Sci. Instrum. **79**, 114901 (2008).
[21] G. Chen and C. L. Tien, J. Appl. Phys. **73**, 3461 (1993).

[22] R. B. Wilson, B. A. Apgar, L. W. Martin, and D. G. Cahill, Opt. Exp. **20**, 28829 (2012).
[23] E. T. Swartz and R. O. Pohl, Rev. Mod. Phys. **61**, 605 (1989).
[24] D. H. Dye, J. B. Ketterson, and G. W. Crabtree, J. Low Temp. Phys. **30**, 813 (1978).
[25] E. Beaurepaire, J.-C. Merle, A. Daunois, and J.-Y. Bigot, Phys. Rev. Lett. **76**, 4250 (1996).
[26] Edited by Y. S. Touloukian, *Thermophysical Properties of High Temperature Solid Materials*, Vol. 1 (Macmillan, New York, 1967).
[27] *American Institute of Physics Handbook*, 3rd ed. (McGraw-Hill, New York, 1972).
[28] M. J. Duggin, J. Phys. D: Appl. Phys. **3**, L21 (1970).
[29] J. A. Birch, W. R. G. Kemp, P. G. Klemens, and R. J. Tainsh, Australian J. Phys. **12**, 455 (1959).